Numerical and experimental modelling of cylindrical tuned liquid dampers

B. Molin, F. Remy, J. Bonnici, J.-B. Lacaze

Aix Marseille Université, CNRS, Centrale Marseille, IRPHE UMR 7342,
13451 Marseille cedex 20, France

I. Introduction

So-called Tuned Liquid Dampers (TLDs) are gaining interest as devices to mitigate the resonant response of slender buildings under wind or earthquake excitation. Some TLDs are of sloshing type, consisting in tanks partly filled with water, with the natural frequency of their first sloshing mode adjusted to the resonant frequency of the structure. Energy dissipation is enhanced by perforated screens. The two-dimensional case of rectangular TLDs has been extensively investigated numerically and experimentally — e.g. see Warnitchai & Pinkaew (1998), Tait (2008), Faltinsen *et al.* (2011), Crowley & Porter (2012) or Molin & Remy (2013).

Figure 1: Considered geometries: circular screen (left) or along a diameter (right).

In the case of axisymmetric buildings such as airport or wind towers TLDs should preferably be axisymmetric as well. Ghaemmaghami *et al.* (2012) have proposed an annular TLD with two horizontal solid baffles at the outer wall. Here we consider cylindrical tanks with vertical perforated screens, either radial or circular, or a combination of both. There are two basic cases: one circular screen or one screen along a diameter, perpendicular to the direction of forced motion (Fig. 1). We have investigated both cases through numerical and experimental modelling.

II. Numerical models

The theoretical frame closely follows Molin & Remy (2013): potential flow theory is assumed with the free surface equations linearized. With the velocity potential written as

$$\Phi(R,\theta,z,t) = A\,\omega\,\Re\left\{\varphi(R,\theta,z)\,\mathrm{e}^{-\mathrm{i}\,\omega t}\right\} \tag{1}$$

where (R,θ,z) are cylindrical coordinates from the bottom of the tank, A is the surge motion amplitude and ω the frequency, the boundary value problem writes

$$\Delta\varphi = 0 \qquad 0 \le R \le b \qquad 0 \le z \le h \tag{2}$$

$$g\,\varphi_z - \omega^2\,\varphi = 0 \qquad z = h \tag{3}$$

$$\varphi_z = 0 \qquad z = 0 \tag{4}$$

$$\varphi_R = \cos\theta \qquad R = b \tag{5}$$

(b the radius of the tank and h the filling height of water).

At the porous screen a quadratic discharge law is assumed (Molin, 2011):

$$P_- - P_+ = \rho\,\frac{1-\tau}{2\,\mu\,\tau^2}\,V_r\,|V_r|, \tag{6}$$

with $P_- - P_+$ the pressure drop, τ the porosity or open-area ratio, μ a discharge coefficient, and V_r the relative velocity of the flow with respect to the screen.

II.1 Circular screen

The velocity potential is written as

$$\varphi_1 = \cos\theta \left\{ \varphi_{NS} + B_0 \frac{J_1(k_0 R)}{k_0\, J_1'(k_0 a)} \frac{\cosh k_0 z}{\cosh k_0 h} + \sum_{n=1}^{\infty} B_n \frac{I_1(k_n R)}{k_n\, I_1'(k_n a)} \cos k_n z \right\} \tag{7}$$

in the inner sub-domain ($0 \le R \le a$), and

$$\begin{aligned} \varphi_2 &= \cos\theta \left\{ \varphi_{NS} + B_0 \frac{Y_1'(k_0 b)\, J_1(k_0 R) - J_1'(k_0 b)\, Y_1(k_0 R)}{k_0\, (Y_1'(k_0 b)\, J_1'(k_0 a) - J_1'(k_0 b)\, Y_1'(k_0 a))} \frac{\cosh k_0 z}{\cosh k_0 h} \right. \\ &+ \left. \sum_{n=1}^{\infty} B_n \frac{I_1'(k_n b)\, K_1(k_n R) - K_1'(k_n b)\, I_1(k_n R)}{k_n\, (I_1'(k_n b)\, K_1'(k_n a) - K_1'(k_n b)\, I_1'(k_n a))} \cos k_n z \right\} \end{aligned} \tag{8}$$

in the annular sub-domain ($a \le R \le b$). In these equations k_0, k_n are the roots of the dispersion equation $\omega^2 = g\, k_0 \tanh k_0 h = -g\, k_n \tan k_n h$ and φ_{NS} stands for the solution in the absence of screen:

$$\varphi_{NS} = A_0 \frac{J_1(k_0 R)}{k_0\, J_1'(k_0 b)} \frac{\cosh k_0 z}{\cosh k_0 h} + \sum_{n=1}^{\infty} A_n \frac{I_1(k_n R)}{k_n\, I_1'(k_n b)} \cos k_n z \tag{9}$$

with $A_0 = 2\, \sinh 2k_0 h / (2\, k_0 h + \sinh 2k_0 h)$, $A_n = 4\, \sin k_n h / (2\, k_n h + \sin 2\, k_n h)$.

Only the discharge equation (6) remains to be verified. The relative flow velocity at the screen is

$$V_r(z,\theta,t) = A\,\omega\, \cos\theta\, \Re\left\{ \left[(\alpha_0 + B_0) \frac{\cosh k_0 z}{\cosh k_0 h} + \sum_n (\alpha_n + B_n) \cos k_n z \right] \mathrm{e}^{-\mathrm{i}\,\omega t} \right\} \tag{10}$$

with $\alpha_0 = A_0\, (J_1'(k_0 a)/J_1'(k_0 b) - 1)$, $\alpha_n = A_n\, (I_1'(k_n a)/I_1'(k_n b) - 1)$, while the pressure drop is

$$P_1 - P_2 = A\,\rho\,\omega^2\, \cos\theta\, \Re\left\{ \mathrm{i} \left[\beta_0\, B_0 \frac{\cosh k_0 z}{\cosh k_0 h} + \sum_n \beta_n\, B_n \cos k_n z \right] \mathrm{e}^{-\mathrm{i}\,\omega t} \right\} \tag{11}$$

and the β_i coefficients have complicated expressions not reproduced here.

The following derivations closely follow Molin & Remy (2013) with Lorentz linearization being applied both to the time and angular coordinate dependencies:

$$\Re\left\{ f\, \mathrm{e}^{-\mathrm{i}\,\omega t} \right\} \left| \Re\left\{ f\, \mathrm{e}^{-\mathrm{i}\,\omega t} \right\} \right| \simeq \frac{8}{3\,\pi} \|f\|\, \Re\left\{ f\, \mathrm{e}^{-\mathrm{i}\,\omega t} \right\} \qquad\qquad \cos\theta\, |\cos\theta| \simeq \frac{8}{3\,\pi} \cos\theta$$

II.1 Screen along a diameter

In the case of a solid wall, Bauer (1963) has proposed a solution written as the solid motion plus a combination of natural modes, that is eigen-functions satisfying an homogeneous Neumann condition at the vertical walls. In the case of a porous wall it turns out to be more handy to use eigen-functions satisfying the linearized free surface condition, alike in the circular case.

That is, in the sub-domains ① and ② of Fig. 1 the velocity potential φ_i is written as

$$\begin{aligned} \varphi_{1,2} &= \sum_{m=0}^{\infty} \cos 2m\theta \left\{ \pm A_{m0} \frac{J_{2m}(k_0 R)}{k_0\, J_{2m}'(k_0 b)} \frac{\cosh k_0 z}{\cosh k_0 h} \pm \sum_{n=1}^{\infty} A_{mn} \frac{I_{2m}(k_n R)}{k_n\, I_{2m}'(k_n b)} \cos k_n z \right\} \\ &+ \sum_{m=0}^{\infty} \cos(2m+1)\theta \left\{ B_{m0} \frac{J_{2m+1}(k_0 R)}{k_0\, J_{2m+1}'(k_0 b)} \frac{\cosh k_0 z}{\cosh k_0 h} + \sum_{n=1}^{\infty} B_{mn} \frac{I_{2m+1}(k_n R)}{k_n\, I_{2m+1}'(k_n b)} \cos k_n z \right\} \end{aligned} \tag{12}$$

In this equation $\pm$ means $+$ in sub-domain ① and $-$ in sub-domain ②. When the screen is solid the B_{mn} coefficients are zero identically. When there is no screen the A_{mn} and B_{mn} coefficients are zero except for the B_{0n} which are identical with the A_n in (9).

There remains to verify the no flow condition at the outer wall and the discharge equation at the porous screen. From the development

$$\cos(2m+1)\theta = \pm\alpha_{m0} \pm \sum_{n=1}^{\infty} \alpha_{mn} \cos 2n\theta \qquad 0 \le \theta \le \pi \tag{13}$$

where, again, $\pm$ means $+$ in subdomain ① and $-$ in subdomain ②, and

$$\alpha_{m0} = \frac{2}{\pi}\,\frac{(-1)^m}{2m+1} \qquad \alpha_{mn} = \frac{4}{\pi}\,\frac{(-1)^{m+n}\,(2m+1)}{(2m+1)^2 - 4\,n^2} \tag{14}$$

the no-flow condition at the outer wall results in

$$A_{mn} + \sum_{p=0}^{\infty} \alpha_{pm}\, B_{pn} = \alpha_{0m}\, B_{0nNS} \qquad m, n = 0, \infty \tag{15}$$

where B_{0nNS} is the No Screen case solution (9). Equivalently, in vector form:

$$\overrightarrow{A} = \mathbf{AB} \cdot \overrightarrow{B} + \overrightarrow{R_A} \tag{16}$$

where $\overrightarrow{A} = (A_{01}, A_{02}, \ldots, A_{0N}, A_{11}, \ldots, A_{MN})$, $\overrightarrow{B} = (B_{01}, B_{02}, \ldots, B_{0N}, B_{11}, \ldots, B_{MN})$ and M, N are the truncation orders of the m and n series. There remains to verify the discharge equation at the screen which takes the form

$$\sum_{m=0}^{\infty} (-1)^m \left\{ A_{m0}\, \frac{J_{2m}(k_0 R)}{k_0\, J'_{2m}(k_0 b)}\, \frac{\cosh k_0 z}{\cosh k_0 h} + \sum_{n=1}^{\infty} A_{mn}\, \frac{I_{2m}(k_n R)}{k_n\, I'_{2m}(k_n b)}\, \cos k_n z \right\}$$

$$= \mathrm{i}\; F(R,z) \left[\sum_{m=0}^{\infty} (2m+1)\,(-1)^m \left\{ B_{m0}\, \frac{J_{2m+1}(k_0 R)}{k_0\, J'_{2m+1}(k_0 b)}\, \frac{\cosh k_0 z}{\cosh k_0 h} + \sum_{n=1}^{\infty} B_{mn}\, \frac{I_{2m+1}(k_n R)}{k_n\, I'_{2m+1}(k_n b)}\, \cos k_n z \right\} - R \right] \tag{17}$$

with

$$F(R,z) = \frac{2}{3\pi}\,\frac{1-\tau}{\mu\tau^2}\,\frac{A}{R^2}\; \times \left\| \sum_{m=0}^{\infty} (2m+1)\,(-1)^m \left\{ B_{m0}\, \frac{J_{2m+1}(k_0 R)}{k_0\, J'_{2m+1}(k_0 b)}\, \frac{\cosh k_0 z}{\cosh k_0 h} + \sum_{n=1}^{\infty} B_{mn}\, \frac{I_{2m+1}(k_n R)}{k_n\, I'_{2m+1}(k_n b)}\, \cos k_n z \right\} - R \right\|$$

Alike in the two-dimensional case an iterative procedure is devised where $F(R,z)$ is given from the previous two steps. Both sides of equation (17) are first multiplied by $\cosh k_0 z / \cosh k_0 h$ (then $\cos k_n z$) and integrated in z from 0 to h. Then they are multiplied by $J_{2p}(k_0 R)/(k_0\, J'_{2p}(k_0 b))$ (then $I_{2p}(k_n R)/\,(k_n\, I'_{2p}(k_n b))$) and integrated in R from 0 to b. In this way one gets the vectorial equation

$$\mathbf{M_A} \cdot \overrightarrow{A}^{(j)} = \mathrm{i}\; \mathbf{M}_B^{(j)} \cdot \overrightarrow{B}^{(j)} + \mathrm{i}\; \overrightarrow{R}_C^{(j)} \tag{18}$$

Combination with (16) yields a linear system in $\overrightarrow{B}$. In the implementation numerical convergence problems were encountered associated with the evanescent components. In the numerical results shown further down in this paper, related to relatively shallow depth cases, the evanescent modes are just neglected.

III. Experiments

Experiments were carried out with the Hexapode bench of Centrale Marseille. The internal diameter of the tank was 0.97 m, the circular screen diameter 0.5 m. In the circular case the screen porosity was 23 %, in the diameter case it was 18 %. The screens had the same thickness, 2 mm, and circular openings with a diameter of 4 mm. Tests were done at 15 cm, 25 cm and 35 cm filling heights. Here we show results at a depth of 25 cm.

The range of frequencies was from 2 through 12 rad/s. When there is no screen, the first natural frequencies (below 12 rad/s) of the sloshing modes are 5.25 rad/s and 10.34 rad/s. With a solid circular screen they are 8.29 rad/s for the inner sub-domain and 4.02 rad/s and 11.67 rad/s for the annular sub-domain. With a solid diameter, they are 7.53 rad/s, 8.64 rad/s, 10.33 rad/s, 11.64 rad/s, 11.90 rad/s.

In the computations the discharge coefficient μ was taken equal to 0.5.

In the circular case, Fig. 2 shows the experimental and numerical added mass (left) and damping (right) coefficients, for different amplitudes of motion.

In the perforated diameter case, Fig. 3 shows the numerical and experimental added mass coefficients, while Fig. 4 shows the damping coefficients.

Good agreement is generally observed between the experimental and numerical hydrodynamic coefficients.

More results, with other screen arrangements, will be shown at the workshop.

References

Bauer H.F., 1963. Liquid sloshing in a cylindrical quarter tank. *AIAA Journal*, **1**, 2601–2606.

Crowley S., Porter R., 2012. An analysis of screen arrangements for a tuned liquid damper. *Journal of Fluids and Structures*, **34**, 291–309.

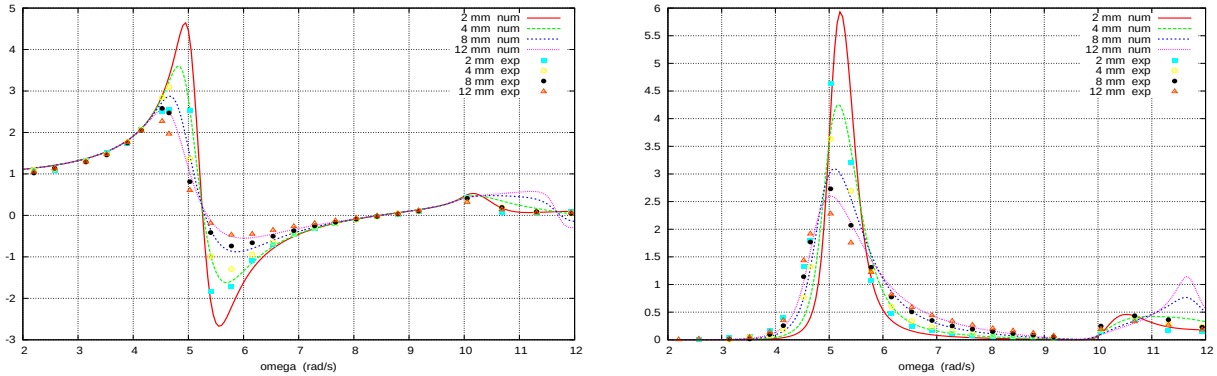

Figure 2: Circular screen. Added mass (left) and damping (right) coefficients.

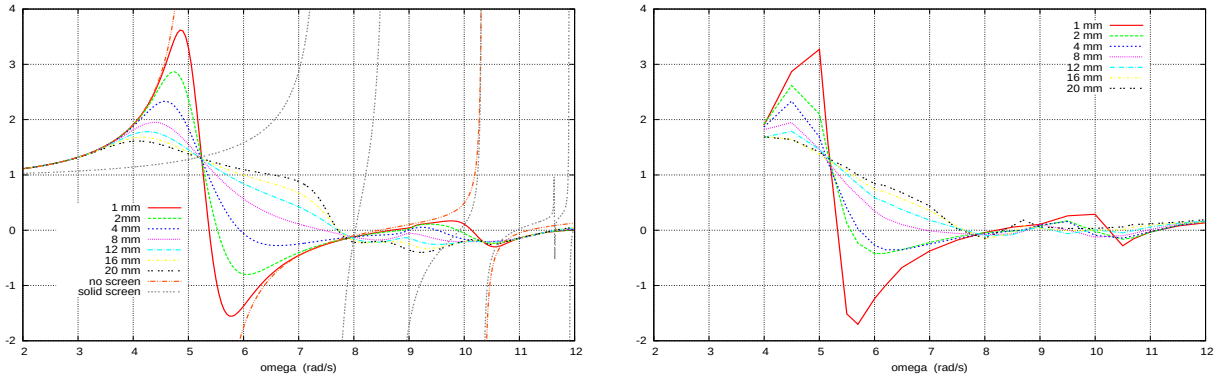

Figure 3: Screen along a diameter. Numerical (left) and experimental (right) added mass coefficients.

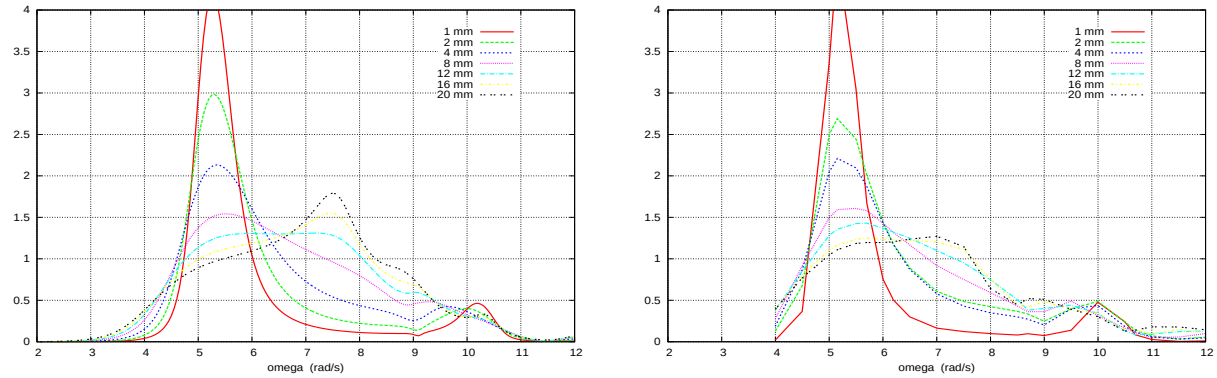

Figure 4: Screen along a diameter. Numerical (left) and experimental (right) damping coefficients.

Faltinsen O., Firoozkoohi R., Timokha A.N., 2011. Steady-state liquid sloshing in a rectangular tank with a slat-type screen in the middle: Quasilinear modal analysis and experiments. *Physics of Fluids*, **23**, 042101.

Ghaemmaghami A.R., Kianoush M.R., Mardukhi J. 2012. Numerical study on annular tuned liquid dampers for controlling the response of wind towers subjected to seismic loads. In *Proc. 15th World Conference on Earthquake Engineering*, Lisbon.

Molin B., 2011. Hydrodynamic modeling of perforated structures. *Applied Ocean Research*, **33**, 1–11.

Tait M.J., 2008. Modelling and preliminary design of a structure-TLD system. *Engineering Structures*, **30**, 2644–2655.

Warnitchai P., Pinkaew T., 1998. Modelling of liquid sloshing in rectangular tanks with flow-dampening devices. *Engineering Structures*, **20**, 593–600.